J Mater Sci (2010) 45:6038–6045
DOI 10.1007/s10853-010-4688-9

In vitro degradation and cell attachment of a PLGA coated biodegradable Mg–6Zn based alloy

J. N. Li · P. Cao · X. N. Zhang · S. X. Zhang · Y. H. He

Received: 10 January 2010 / Accepted: 1 June 2010 / Published online: 15 June 2010

Abstract Currently available engineering magnesium alloys have several critical concerns if they are about to be used as biomaterials, particularly the concern about the toxicity of the common alloying elements such as aluminum and rare earth (RE). There is an increasing demand to develop new magnesium alloys that do not contain any toxic elements. It is also desirable, yet challenging, to develop such a material that has a controllable degradation rate in the human fluid environment. This paper presents mechanical properties, degradation, and in vitro cell attachment of a newly developed Mg–6Zn magnesium alloy. The alloy demonstrated comparable mechanical properties with typical engineering magnesium alloys. However, the bare alloy did not show an acceptable corrosion (degradation) rate. Application of a polymeric PLGA or poly(lactide-*co*-glycolide) coating significantly decreased the degradation rate. The results obtained from cell attachment experiments indicated that the mouse osteoblast-like MC3T3 cells could develop enhanced confluence on and interactions with the coated samples.

J. N. Li · X. N. Zhang (✉) · S. X. Zhang
School of Materials Science and Engineering, Shanghai Jiao Tong University, Shanghai 200240, People's Republic of China
e-mail: xnzhang@sjtu.edu.cn

P. Cao (✉)
Department of Chemical and Materials Engineering, the University of Auckland, Private Bag 92019, Auckland 1142, New Zealand
e-mail: p.cao@auckland.ac.nz

Y. H. He
Institute of Powder Metallurgy, Central South University, Changsha 410083, People's Republic of China

Introduction

Historically, corrosion has been thought to be a critical issue that should be controlled to a level as minimal as possible for structural materials. In recent years, there has been a paradigm shift in thinking in the biomaterial community in terms of corrosion. There is now increasing interest in intentionally using a corrodible alloy in some medical device applications such as intravascular stents and orthopedic implants [1] because the use of biodegradable materials can avoid a second surgery. In this case, the human body must be able to deal with the corrosion products and their effects. There are three major groups of biodegradable metallic biomaterials: (1) iron and its alloys (Fe–Mn) [2–4], (2) magnesium (Mg) and its alloys [5–8], and (3) tungsten (W) [9]. Magnesium has attracted a great deal of interest due to its exceptional mechanical and physiological features. Physiologically, Mg^{2+} ions are a cofactor in many enzymatic reactions and essential for normal neurological and muscular functions. Also, the presence of magnesium benefits the mineralization process of bony tissue and is important to bone's strength and health [10]. An adult human body contains approximately 30 g of magnesium in muscle and bone [11] and also need to take in 420 mg/day. From the perspective of physical and mechanical features, magnesium has good compatibility with human bone. For example, its density of 1.74 g/cm^3 and Young's modulus of 41–45 GPa are close to natural bone (1.8–2.1 g/cm^3 and $\sim$30 GPa, respectively). Advantageous over inorganic and polymeric biomaterials, Mg has much higher fracture toughness and yield strength. Even more important and attractive is its biodegradability. Current surgical orthopedics requires a secondary surgical procedure to remove the orthopedic plate, screw, or pin after the tissue has healed sufficiently. But if these

orthopedic tools are made of magnesium, instead of stainless steel or titanium, then they can naturally degrade in, and be excreted from, the human body and therefore the secondary surgery can be avoided.

The potential application of magnesium in orthopedics was realized in the early twentieth century. The first surgical attempt was reported by Lambotte in 1907 [12], but it was not successful because the pure magnesium metal corroded too rapidly in vivo, losing its mechanical integrity only 8 days after surgery and leaving hydrogen gas pockets beneath the skin. As such, the use of magnesium in orthopedic devices was quickly abandoned. Attempts at using magnesium were spurred again in the 1940s [12] and subsequently boosted in the early 2000s, in line with the advancement and development of magnesium technologies. The past few years have seen a big leap in the development of magnesium biomaterials [1, 13]. Magnesium metal stents (e.g. AMS, Biotronik GmbH) have moved to the clinical arena [4, 14, 15]. With the success of the clinical experiments, it is envisaged that biodegradable Mg will attract more academic investigations and capital investment.

In the development of biometallic alloys and design of biomedical devices, alloy compositions must be carefully chosen; the potential toxicological elements should be ideally avoided if possible. In this regard, high purity unalloyed magnesium is an ideal candidate because it does not contain any other alloying elements and it does have the lowest degradation rate [16] (note here that in the magnesium community "high purity" means extremely low concentrations of Fe, Cu, and Ni, e.g., <40 ppm Fe, <20 ppm Ni, and <20 ppm Cu). Unfortunately, the pure Mg does not show an acceptable mechanical strength. Most engineering Mg alloys, which are being considered for biomedical applications, contain aluminum (e.g., AZ series alloys) and/or rare earth (RE). Aluminum is known to be harmful to neurons [17] and osteoblasts [18] and its accumulation is associated to dementia and Alzheimer disease [17]. The administration of RE could lead to hepatotoxicity [19]. It is demanding yet challenging to develop biocompatible magnesium with controllable degradation.

Rapid degradation is an intrinsic response of magnesium alloys to chloride containing solutions including body fluid and blood plasma, through the following electrochemical reactions:

$$Mg(s) + 2H_2O \rightarrow Mg(OH)_2 + H_2(g) \quad (1)$$

$$Mg(OH)_2(s) + 2Cl^- \rightarrow MgCl_2(\text{soluble}) + 2OH^- \quad (2)$$

The local alkalization due to the formation of OH^- ions and the build-up of hydrogen gas are harmful to the surrounding tissue and also affect the pH-dependent physiological reaction balances [16]. Therefore, an initially low degradation rate, or ideally a controllable degradation rate, is desirable to avoid further deterioration of the adjacent tissue. In order to reduce the degradation rate, a typical approach is to apply a protective coating on Mg (the other two methods are purification and alloying). A coating, when used to reduce and/or retard degradation in the human body, should be also biocompatible per se. A number of coating technologies are available or under development, such as conversion coatings, anodizing, micro-arc oxidation, and polymeric coatings [13].

In this paper, we used a model magnesium Mg–6 wt%Zn alloy (designated Mg–6Zn alloy hereafter). We chose Zn as the main alloying element in the alloy design because: (1) Zn is an essential element in the human body; (2) Zn is a common alloying element for improving the mechanical properties of magnesium alloys; and (3) alloying with Zn has been reported to reduce the corrosion rate of magnesium alloys in both simulated body fluid (SBF) and Hank's solution [20] and to increase cell viability [20]. Although excess zinc exposure is toxic [21], the risk of a high-Zn content magnesium can be offset if the material's degradation rate can be significantly reduced. For example, recently Zberg et al. [22] reported ternary Mg–Zn–Ca (Zn content up to 35 at.%) in the form of metallic glasses. These glassy alloys show good tissue biocompatibility but without hydrogen evolution. We employed a PLGA—poly(lactide-*co*-glycolide)—coating on the Mg alloy samples to reduce their degradation rate. PLGA copolymers are among the few approved synthetic polymers for human clinical applications due to their excellent biocompatibility. They are also biodegradable through a simple hydrolysis of the ester bonds into lactic and glycolic acid, which are excreted by normal metabolic pathways [23]. Furthermore, PLGA can be easily processed and their physical, mechanical, chemical, and degradative properties can be engineered by adjusting the ratio of the two co-monomers [24]. A simple dipping technology was used to prepare PLGA coatings on the magnesium alloy samples. We reported on their mechanical properties, degradation, and in vitro cell attachment behavior of the Mg–6Zn alloy.

Experimental procedure

Material preparation

Magnesium alloy samples with a nominal composition of Mg–6 wt%Zn were prepared from high purity Mg (>99.99 wt%) and high purity Zn (>99.999 wt%) ingots. The ingots were melted at 750 °C under a protective cover gas. The as-cast bars were solid solutionized at 350 °C for 2 h (water quenching). Subsequently, the bars were extruded at 250 °C with an extrusion ratio of 8:1 (air

cooling). Cylindrical tensile test samples (gauge length 35 mm, diameter 6 mm) were machined from the as-extruded bars with tensile stress parallel to the extrusion direction.

Immersion disk samples were sliced from the as-extruded bars. Prior to dipping, each disk sample (11.3 mm diameter) was ground up to 1200 grit, followed by ultrasonic cleaning in acetone and rinsing with ethanol and distilled water. PLGA solution for dipping coating was prepared by dissolving PLGA powder (average molecular weight $M\text{w} = 140{,}000$, co-polymer ratio = 90:10) in chloroform solvent. The PLGA concentrations were 2 and 4 wt%. The sliced disk samples were then dipped and pulled out. Coatings formed when the solvent evaporated and PLGA solidified. The mass gains were recorded in order to evaluate the coating thickness.

Microstructure characterization and mechanical tests

Microstructural observations were made for the as-extruded and as-coated samples, using a Jeol JSM 6460 scanning electron microscope (SEM, at an accelerating voltage of 20 kV). Tensile tests were performed at room temperature with a universal tensile testing machine at a constant crosshead speed of 0.5 mm/min.

Electrochemical measurement

A three-electrode cell was used for electrochemical measurements using a PARSTAT 2273 electrochemical system (Princeton Applied Research, USA). Platinum was used as the counter electrode while saturated calomel electrode (SCE) as the reference. A working area of 1 cm^2 was exposed to the electrolyte. Potentiodynamic polarization curves were measured at a scan rate of 1 mV/s. The corrosion properties were obtained from the potentiodynamic polarization curves as per the ASTM standard G102. All the measurements were made in a 0.9% NaCl solution at 37 ± 0.5 °C. The corrosion potential and current density is calculated with the Parstat software package, based on Tefel extrapolation. Electrochemical impedance spectroscopy (EIS) analysis was also performed in a 0.9% NaCl solution. The amplitude of the sinusoidal perturbing signal was 5 mV, and the frequency varied from 100 kHz to 200 Hz for the coated samples and from 100 kHz to 0.1 Hz for the bare alloy. Prior to the EIS measurements, the Mg electrode was immersed in the electrolytic unit until a steady open-circuit potential value was reached.

Immersion test

Immersion tests were carried out conforming to the ASTM standard G31. Each sample was immersed in a 100 mL 0.9% NaCl solution separately. The temperature of the solution was controlled at 37 ± 0.5 °C with a water bath. After prescribed immersion times, the samples were rinsed with distilled water, acetone, and a chromic acid (180 g/L Cr_2O_3) to remove the corrosion products and/or the residual coating on the surface. The samples were then quickly washed with distilled water and dried again, and the final weight was recorded according to ASTM standards G1 and F1635. The weight loss (R) was used to calculate the degradation rate of the alloys by the formula $R = \Delta W/(A \times T)$, where ΔW is the weight loss (mg), A is the exposed area of the samples (cm^2), and T is the exposure time (h).

Cell culture test

Disk samples with and without PLGA coatings were first sterilized by ethylene oxide gas before being subjected to cell culture. The mouse osteoblast-like cells MC3T3-E1 (Committee on Type Culture Collection of Chinese Academy of Sciences) were cultured in Dulbecco's modified Eagle's medium (DMEM, Gibco), supplemented with 10% fetal bovine serum (FBS) in a humidified incubator of 95% relative humidity and 5% CO_2 at 37 °C. At confluence, the cells were harvested, counted, and reseeded on the surface of the Mg specimens. After the prescribed time period (72 h in this study), the Mg substrates were rinsed with phosphate-buffered saline (PBS) to remove any non-adherent cells. The remaining cells seeded on the magnesium specimens were fixed in an immobilization solution of 2.5% glutaraldehyde for 30–60 min at 4 °C. They were then post-fixed in an osmium tetroxide solution (OsO_4, 1%) for 90–120 min at 4 °C. The cells were dehydrated through sequential washings in 30, 50, 70, 90, 95, and 100 vol% ethanol series. Specimens were then critical point dried and sputtered with gold for SEM examination. The osteoblast morphology and the adhesion location on the Mg substrates of interest were examined using a FEI Test 0625 field-emission SEM at an accelerating voltage of 20 kV.

Results

Microstructures and mechanical properties

Figure 1 presents the typical microstructures observed in the as-extruded alloy, showing a uniform and fine grained equiaxed microstructure (grain size about 30 μm). Neither bulky precipitates nor impurities were found. The chemical analysis shows a low impurity level of all major impurities, e.g., 38 ppm Fe and 5 ppm Ni (the impurity levels for other elements such as Si, Cu, Al, and Mn has been reported in Ref. [25]). Mechanical testing results [25] show that the current Mg–6Zn alloy exhibits comparable yield strength

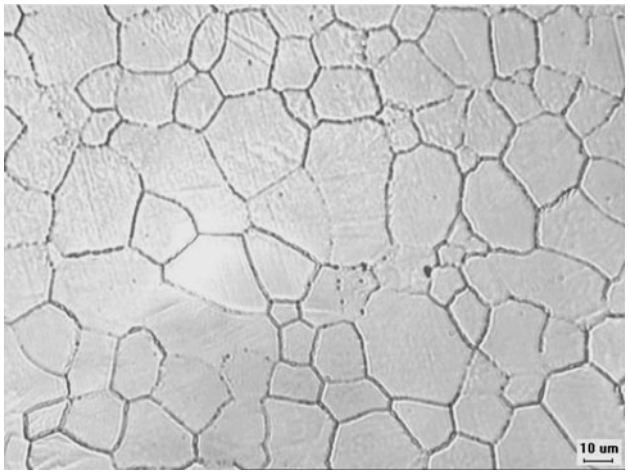

Fig. 1 Optical micrographs showing the microstructures of as-extruded Mg6Zn alloy

and Young's modulus to other Mg alloys, e.g., Mg–Ca and Mg–Mn–Zn [26, 27].

SEM images revealed a dense and continuous PLGA coating on the Mg substrates (Fig. 2a, c). The estimated coating thickness, from Fig. 2b, d, was 33 ± 5 and 72 ± 5 μm for dipping in 2 and 4% solutions, respectively. This is confirmed from the measured weight increments of these two samples, being 1.1 ± 0.1 and 2.8 ± 0.1 mg, respectively. As expected, the coating did not affect the mechanical properties of the Mg substrates.

Electrochemical potentiodynamic polarization curves

Figure 3 shows typical polarization curves of the two Mg–6Zn alloy samples with different coating thicknesses in the 0.9% NaCl solution. For comparison, the polarization curve for the uncoated Mg6Zn alloy sample was also included in Fig. 3. Generally, the cathodic polarization curve represents the cathodic hydrogen evolution while the anodic one represents the dissolution of Mg. Table 1 summarizes the corrosion potential (E_{corr}) and corrosion current density (i_{corr}) obtained by Tafel extrapolation. The E_{corr} value of the Mg–6Zn is less negative than that of pure Mg [28], indicating that Mg6Zn alloy is less susceptible to corrosion. This is mainly because of the much lower impurity level in the present alloy than in commercial pure Mg (e.g. commercial pure Mg contains ~200–300 ppm Fe) and also the Zn alloying effect. Furthermore, the E_{corr} values indicate that the two coated samples are slightly nobler than the bare alloy, but the i_{corr} values for these two coated samples are much lower, as compared to the bare alloy by at least two orders of magnitude. A breakdown potential (E_{bd}) appeared in the anodic branch of the polarization curve for the 2% PLGA coating, indicating the destruction of the protective films at the later stage of the experiment. The value of E_{bd} of −1.3 V here is higher than the reported E_{bd} of magnesium alloy in a similar solution (about −1.55 V) [29]. The above results show that the PLGA coatings protect the Mg substrates.

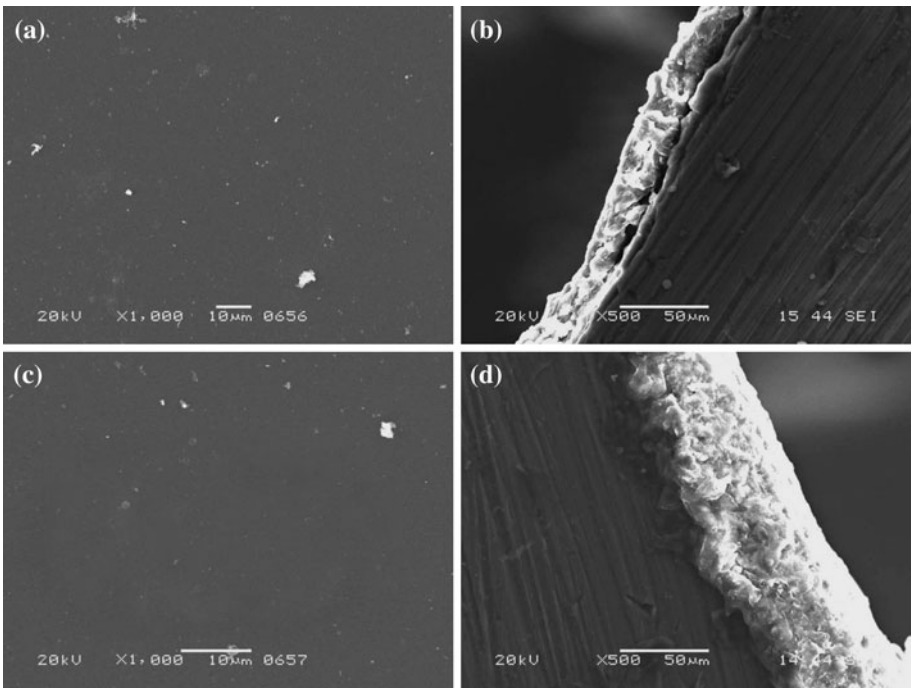

Fig. 2 SEM images of the PLGA coatings. **a**, **b** The surface and cross section of the 2% PLGA sample and **c**, **d** the surface and cross section of the 4% PLGA. The coatings were made from the two different PLGA concentrations in chloroform therefore had different thicknesses

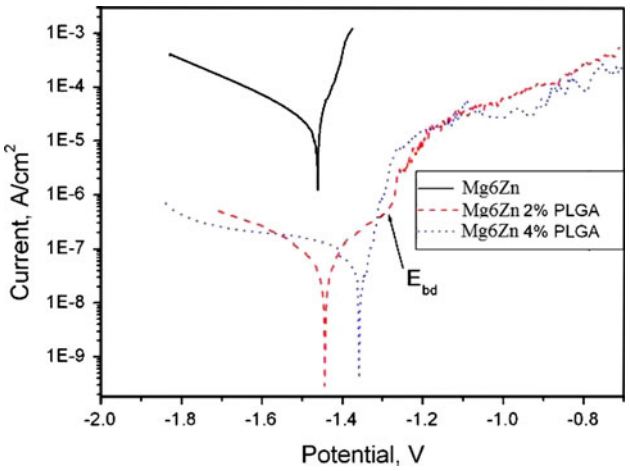

Fig. 3 Polarization curves of uncoated and coated Mg–6Zn samples in 0.9% NaCl solution

Table 1 Corrosion potential and current density of the Mg6Zn alloy samples with and without PLGA coating in 0.9% NaCl solution

	Uncoated Mg6Zn	With 2% PLGA	With 4% PLGA
E_{corr} (V)	−1.46	−1.44	−1.36
i_{corr} (μA cm^{-2})	26.5	0.085	0.097

EIS

Figure 4 presents typical Nyquist diagrams of EIS for the two coating samples (Fig. 4a) and the uncoated sample (Fig. 4b) in the test solution. The bare sample (Fig. 4b) shows a much lower Z_{re} value compared to the coated samples. It also shows a simple semicircle-like curve, consisting of a capacitive loop in the high-frequency regime and a trail of inductive loop in the low-frequency regime. This observation is similar to that of AZ91 alloy in 1 M NaCl solution [30]. The high-frequency capacitive loop reflects charge transfer and the corrosion products formation, while the low-frequency inductive loop relates to relaxation process and also probably to pit formation. In comparison, the EIS curves for the coated samples change dramatically from a simple semicircle to a more complex shape—a Warburg-like portion in the low-frequency regime (Fig. 4a). Further, the Z_{re} values are much higher than the bare sample. This result is similar to that reported for sand blasted mild steel coated with a 30 μm thick layer of fluoropolymer [31].

Immersion corrosion behavior

Figure 5 shows the weight loss of the Mg6Zn alloy samples after different processes. Table 2 summarizes the average degradation rates derived from Fig. 5. The initial degradation rate (measured in the first 72 h) of ~0.06 mg/cm^2/h for the bare sample is similar to that reported for AZ91 [16] and Mg–1Ca [26] but slightly higher than LAE442 [7]. By

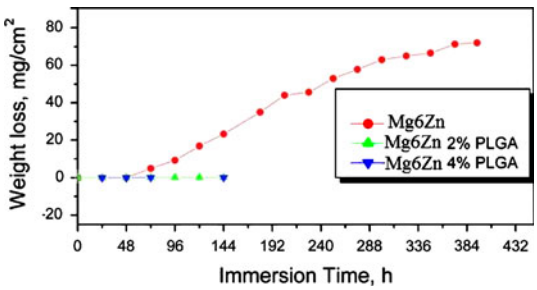

Fig. 5 Weight loss in 0.9% NaCl solution of the Mg6Zn samples: uncoated, with 2% PLGA coating and 4% PLGA coating

Table 2 Average degradation rate of the Mg6Zn alloy samples after 72 h and 144 h of immersion test in 0.9% NaCl solution, in mg/cm^2/h

Degradation rate	Uncoated	With 2% PLGA	With 4% PLGA
72 h	0.063	2.44×10^{-4}	5.61×10^{-4}
144 h	0.161	3.23×10^{-4}	5.62×10^{-4}

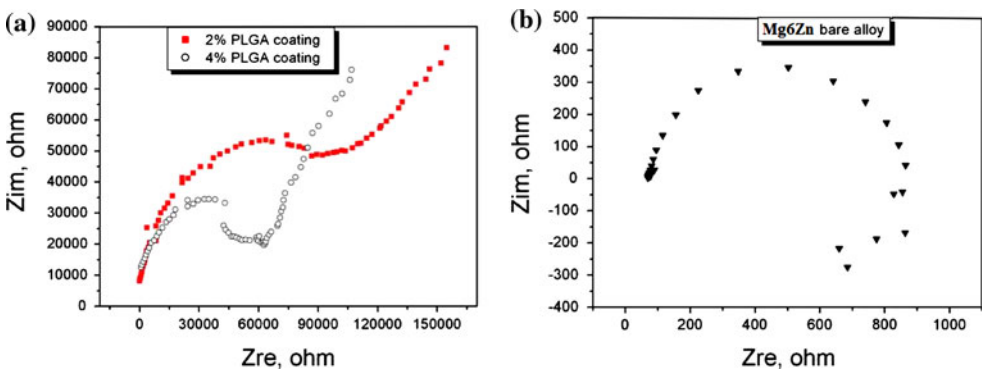

Fig. 4 EIS of **a** the coated and **b** the uncoated Mg6Zn samples

contrast, the coated sample exhibited a significantly reduced degradation rate, by at least two orders of magnitude lower than the bare alloy.

Cell attachment

Figure 6 presents the FE-SEM images of the adhesion and attachment of mouse osteoblast-like MC3T3-E1 on the bare and coated samples. No obvious osteoblast cell attachment was observed on the surface other than coralloid depositions (Fig. 6d–f), although we cannot exclude the probability that some cells were buried in the large number of depositions that make them indiscernible. In contrast, clear osteoblasts spread can be observed on the surface of the coated samples. After 1 day of incubation, many osteoblasts adhered to the surface and displayed a lamellirostral or elongated morphology without preferred directions (Fig. 6a). After 2 days of incubation, fine and long filopodia protrusions were clearly observed, displaying spindle-like morphology with digitations as shown in Fig. 6b. Unlike the bare samples, osteoblast-like cells MC3T3-E1 attached to the PLGA coated alloy formed a cellular entity, which exhibited a flat morphology after 3 days of incubation (Fig. 6c). It can be seen from Fig. 6c that a large number of cells were confluent and interacted with each other completely. The confluence of osteoblast cells led to the formation of dense cell coverage, enveloping the existing pits observed in Fig. 6b. The results indicated that the cells on the coated samples spread extensively and the interactions between the cells/substrate

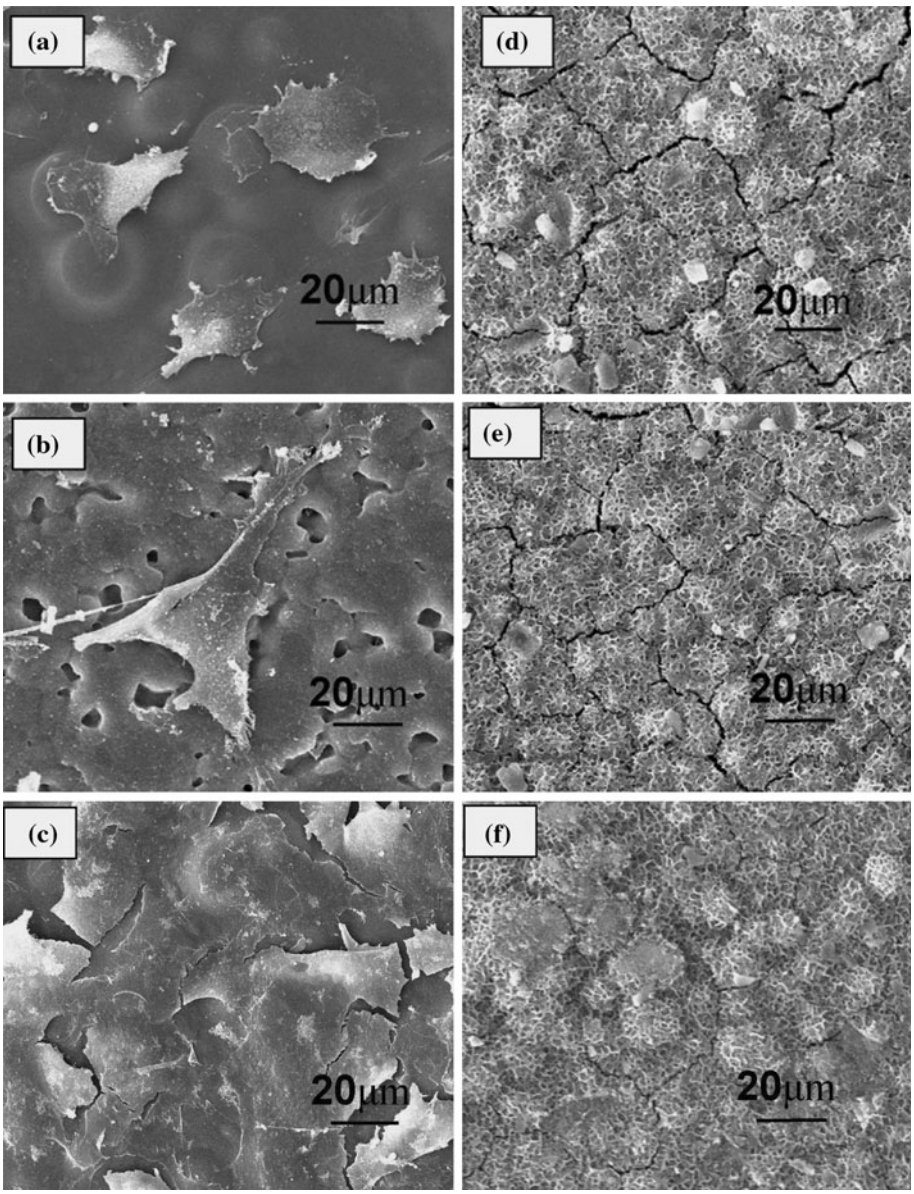

Fig. 6 FE-SEM micrographs of cell morphology after different culture times, **a** 1 day culture, 2% PLGA coating, **b** 2 days culture, 2% PLGA coating, **c** 3 days culture, 2% PLGA coating, **d** 1 day culture, uncoated, **e** 2 days culture, uncoated and **f** 3 days culture, uncoated

and the cell/cell, which are evidenced by the protrusions of lamellipodia and filopodia. In summary, the PLGA coated Mg alloy is more suitable for the cell adhesion and attachment than the bare samples.

Discussion

Degradation behavior of magnesium alloys with PLGA coating

The corrosion potential of the coated samples is elevated slightly, while the corrosion current is reduced significantly, as compared to the bare Mg samples. The improvement of corrosion resistance with the PLGA coatings is further confirmed by the immersion test, as shown in Fig. 5. According to the chemisorption model proposed by Yfantis et al. [32], the monomers—either lactide or glycolide or both—stabilizes the structure of the surface oxides and hence improves corrosion resistance.

An uncommon observation is made in this study: the 2% PLGA coating (about 33 μm thick) performs better than the 4% PLGA coating (about 72 μm thick). We speculate that the thick coating has a poorer quality (e.g. more flaws and voids) than the thin coating. The passivation region on the polarization curves of the 2% PLGA coated sample reveals the passivation behavior on the anodic branch. However, no obvious passivation behavior was observed of the polarization curves on the 4% PLGA coated sample (Fig. 3). It is therefore suggested that the 2% PLGA (thin) coating provides sufficient protection to the sample surface, while the 4% PLGA (thick) coating cannot. The immersion data (Fig. 5) and EIS curves further confirm this speculation: the 2% coating sample shows a larger capacitive semicircle in the high-frequency regime than the 4% coating sample (Fig. 4). Further investigations on the coating microstructures are under way.

Hanzi et al. [33] proposed a model to elucidate the mechanism by which the oxidized coating retards the onset of corrosion and changes the corrosion mode. This model can be adapted here to explain the experimental observations. For a bare alloy (without the PLGA coating), corrosion commonly follows a parabolic law over time since it is a diffusion-controlled process (Fig. 7a). When a coating is applied, the magnesium material obeys a sigmoidal corrosion law (Fig. 7a). Initially, a very low degradation rate is observed due to the protective effect of the coating, which covers the whole surface of the samples (Fig. 7b). The polarization and EIS curves (Figs. 3, 4) indicate the formation of protective films at the early stage. When the degradation process progresses, the protective layer starts to break down. Once the breakdown occurs, the fresh reactive surface exposed to the corrosion medium increases

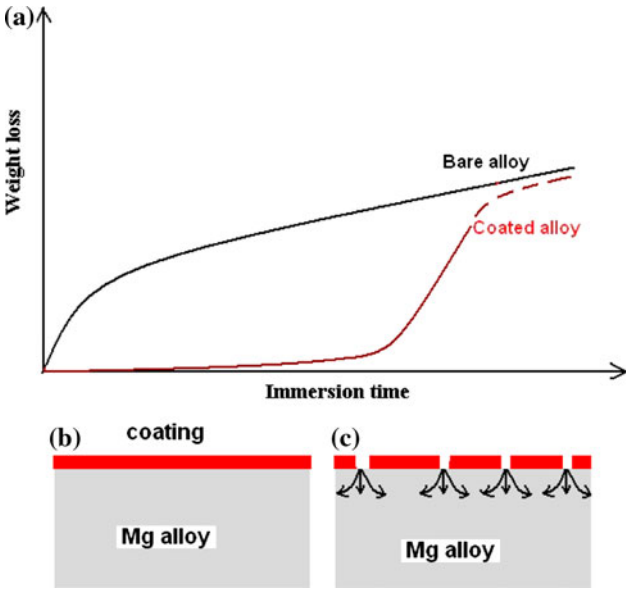

Fig. 7 **a** Schematic degradation diagram showing the degradation performance of the uncoated (bare) and the coated magnesium alloy; **b** initial surface condition of the coated magnesium alloy, and **c** penetrated polymeric coating upon degradation; after the onset of coating breakdown, the reactive area exposed increases

(Fig. 7c) and degradation accelerates. The acceleration of degradation can be supported from the presence of breakdown potential in Fig. 3. Afterwards, the deposition of the corrosion products (self-passivation) in turn acts a barrier to further degradation. The two competing processes—breakdown of the protective layer and self-passivation—persist until most of the protective coating is consumed.

Cell attachment

Cell adhesion, spreading, and migration on substrates are the first sequential reactions when cells come into contact with a material surface and therefore crucial for cell survivals. Cellular behavior and response to biomaterials is an important factor for evaluation of the material's biocompatibility [34]. The results observed in this study clearly demonstrate that the osteoblast cells have been well spread on the coated Mg samples. By contrast, no obvious cell attachment was observed on the surface of uncoated magnesium samples. Extensive spreading and attachment of the osteoblast-like cells MC3T3-E1 illustrates that the PLGA coatings have the ability of improving cell adhesion and further improving the subsequent cellular reactions.

It should be pointed out that more extensive investigation needs to be undertaken with the aim of studying the long term degradation behavior of the materials in vitro and in vivo. Particularly, it is very important to investigate the influence of the coating thickness on the biological performance in order to optimize the dipping process. To be a

practically useful coating, the coating itself should have a sufficient hardness and also provide bonding with the magnesium alloy substrates. Ideally, the coating should be self-healing. It is also noted that with the application of a polymeric coating, it is possible to integrate a drug delivery unit into the coating, which releases some anti-inflammatory medicine during the coatings' degradation process.

Conclusions

In this study, we investigated the mechanical properties, in vitro degradation, and cell attachment of a Mg–Zn based magnesium alloy. The effect of PLGA coating was also studied. The following conclusions can be drawn:

(1) The mechanical properties and degradation of the developed Mg–6Zn magnesium alloy are comparable to cast and wrought magnesium alloys.
(2) The PLGA coating significantly reduces the degradation rate of the magnesium biomaterials, evidenced by the immersion test, potentiodynamic analysis, and EIS measurement.
(3) The coated magnesium alloy samples show significantly enhanced ability of cell attachment compared to the bare magnesium.

Acknowledgements The authors would like to acknowledge the financial support from the National Natural Science Foundation of China (No. 30772182 and No. 30901422), the Shanghai Jiao Tong University Interdiscipline Research Grant (No. YG2009MS53) and the "863" High-tech Programs of China (No. 2009AA03Z424). The useful and constructive comments from the reviewers are acknowledged. PC would also like to acknowledge the financial support from the Foundation of Research Science and Technology (FRST), New Zealand.

References

1. Williams D (2006) Med Device Technol 17:9
2. Mani G, Feldman MD, Patel D, Agrawal CM (2007) Biomaterials 28:1689
3. Peuster M et al (2006) Biomaterials 27:4955
4. Mueller PP, May T, Perz A, Hauser H, Peuster M (2006) Biomaterials 27:2193
5. Heublein B, Rohde R, Kaese V, Niemeyer M, Hartung W, Haverich A (2003) Heart 89:651
6. Song G, Song S (2007) Adv Eng Mater 9:298
7. Witte F, Fischer J, Nellesen J, Crostack H, Kaese V, Pischd A (2006) Biomaterials 27:1013
8. Witte F, Kaese V, Switzer H, Meyer-Lindenberg A, Wirth CJ, Windhag H (2005) Biomaterials 26:3557
9. Peuster M, Fink C, Schnakenburg CV (2003) Biomaterials 24:4057
10. Zreiqat H, Valenzuela SM, Nissan BB, Roest R, Knabe C, Radlanski RJ, Renz H, Evans PJ (2005) Biomaterials 26:7579
11. Saris NL, Mervaala E, Karppanen H, Khawaja JA, Lewenstam A (2000) Clin Chim Acta 294:1
12. Staiger MP, Pietak AM, Huadmai J, Dias G (2006) Biomaterials 27:1728
13. Zeng R, Dietzel W, Witte F, Hort N, Blawert C (2008) Adv Eng Mater 10:B3
14. Erbel R, Di Mario C, Bartunek J, Bonnier J, de Bruyne B, Eberli FR, Erne P, Haude M, Heublein B, Horrigan M, Llsley C, Bose D, Koolen J, Luscher TF, Weissman N, Waksman R (2007) Lancet 369:1869
15. Hotz K, Murphy A (2006) Drug-eluting and absorbable stents push interventional frontiers. The American College of Cardiology. http://eurekalert.org/pub_release/2006-03/acoc-daa031206.php. Accessed 10 June 2010
16. Song G (2007) Corros Sci 49:1696
17. El-Rahman SSA (2003) Pharmacol Res 47:189
18. Ku C-H, Pioletti DP, Browne M, Gregson PJ (2002) Biomaterials 23(6):1447
19. Yumiko N, Yukari T, Yasuhide T, Tadashi S, Yoshio I (1997) Fundam Appl Toxicol 37:106
20. Gu X, Zheng Y, Cheng Y, Zhong S, Xi T (2009) Biomaterials 30:484
21. Yuen CK, Ip WY (2010) Acta Biomater 6:1808
22. Zberg B, Uggowitzer PJ, Loffler JF (2009) Nat Mater 8:887
23. Göpferich A (1996) Biomaterials 17:103
24. Athanasiou KA, Niederauer GG, Agrawal CM (1996) Biomaterials 17:93
25. Zhang S, Zhang X, Zhao C, Li J, Song Y, Xie C, Tao H, Zhang Y, He Y, Jiang Y, Bian Y (2010) Acta Biomater 6:626
26. Li Z, Gu X, Lou S, Zheng Y (2008) Biomaterials 29:1329
27. Zhang E, Yin D, Xu L, Yang L, Yang K (2009) Mater Sci Eng C 29:987
28. Song G, Atrens A, Stjohn D, Nairn J, Li Y (1997) Corros Sci 39(5):855
29. Hara N, Kobayashi Y, Kagaya D, Akao N (2007) Corros Sci 49:166
30. Song G, Atrens A, Wu X, Zhang B (1998) Corros Sci 40:1769
31. Bonora PL, Deflorian F, Fedrizzi L (1996) Electrochim Acta 41:1073
32. Yfantis A, Paloumpa I, Schmeiber D, Yfantis DY (2002) Surf Coat Technol 151–152:400
33. Hanzi AC, Gunde P, Schinhammer M, Uggowitzer PJ (2009) Acta Biomater 5:162
34. Cai K, Rechtenbach A, Hao J, Bossert J, Jandt KD (2005) Biomaterials 26:5960